Inorganic Chemistry

Article

pubs.acs.org/IC

On the Influence of the Vacancy Distribution on the Structure and Ionic Conductivity of A-Site-Deficient $Li_xSr_xLa_{2/3-x}TiO_3$ Perovskites

Wilmer Bucheli,[†] Teresa Durán,[‡] Ricardo Jimenez,[†] Jesús Sanz,*[,†] and Alejandro Varez[‡]

[†]Instituto de Ciencia de Materiales de Madrid (ICMM), CSIC, 28049 Cantoblanco, Madrid, Spain

[‡]Departamento Ciencia e Ingeniería de Materiales, Universidad Carlos III de Madrid, 28911 Leganés, Madrid, Spain

ABSTRACT: The crystal structure and dielectric properties of slowly cooled A-site-deficient perovskites $Li_xSr_xLa_{2/3-x}\square_{1/3-x}TiO_3$ ($0.04 \leq x \leq 0.33$) have been investigated by powder X-ray diffraction (XRD), impedance spectroscopy, and ^{7}Li NMR techniques. In this series, nominal vacancies decrease with Li content, but the total amount of A-site vacancies, n_t = Li + □, participating in conduction processes remains basically constant. Rietveld analysis of the XRD patterns showed a change of symmetry from orthorhombic to tetragonal when the lithium and strontium contents increased above x = 0.08 and from tetragonal to cubic above x = 0.16. Structural modifications are mainly due to the cation vacancy ordering along the c axis, which disappear gradually when the lithium content increases. In agreement with the structural information, two lithium signals with different quadrupole constants are detected in ^{7}Li NMR spectra of orthorhombic/tetragonal phases, which have been associated with lithium in two crystallographic z/c = 0 and $^1/_2$ planes of perovskites. In cubic samples, only a single narrow component, indicative of mobile species, was detected. Lithium motion was thermally activated, with activation energies going from 0.35 to 0.38 eV. Evolution of the bulk dc-conductivity preexponential factors along the series showed a maximum that has been first related to the dependence of lithium hopping on the lithium and vacancy concentrations. Finally, changes in the vacancy ordering, produced along the series, affect the dimensionality of the conductivity, indicating that not only the amount of vacancies but also its distribution are relevant.

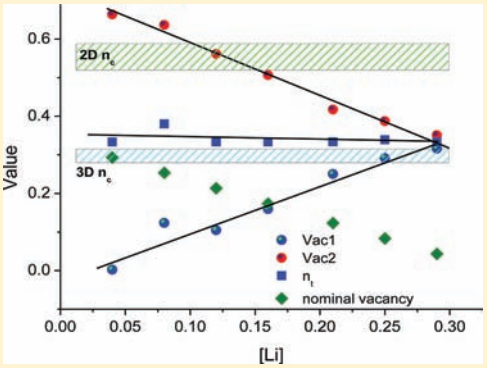

1. INTRODUCTION

Interest in perovskites of the system $Li_{3x}La_{2/3-x}TiO_3$ (LLTO) arose after the discovery of its high ionic conductivity (10^{-3} S cm^{-1} at 300 K), which makes them good candidates for electrochemical devices.[1,2] This system has been extensively studied, and the structural characteristics that promote lithium mobility have been largely analyzed. In these perovskites, La^{3+} ions can be replaced by Li^+ ions, and nominal vacant A sites are given by the expression □ = $^1/_3 - 2x$ (line 1 in Figure 1). In orthorhombic perovskites, $x < 0.06$, vacancies are disposed in alternate planes, favoring the two-dimensional (2D) mobility of lithium.[3−5] In samples with higher lithium contents ($x > 0.1$), the ordering of the vacancies decreases and the structure becomes tetragonal.[5] Finally, in lithium-rich samples quenched from high temperature, a pseudocubic rhombohedral phase is favored[6−8] where vacancy ordering is removed. In this case, Li ions display a three-dimensional (3D) mobility.

In LLTO compounds, a large number of chemical substitutions on A and/or B sites of the perovksite have been studied to improve conductivity or to understand high Li-ion mobility.[9] However, up to now, structural factors that improve ion conductivity are not well established. In particular, the influence of A-site vacancies or the expansion of the unit cell on lithium conductivity is not clear. For instance, the substitution of Ti by pentavalent ions, like Nb and Ta, produces a large number of vacant A sites and an expansion of the unit cell;

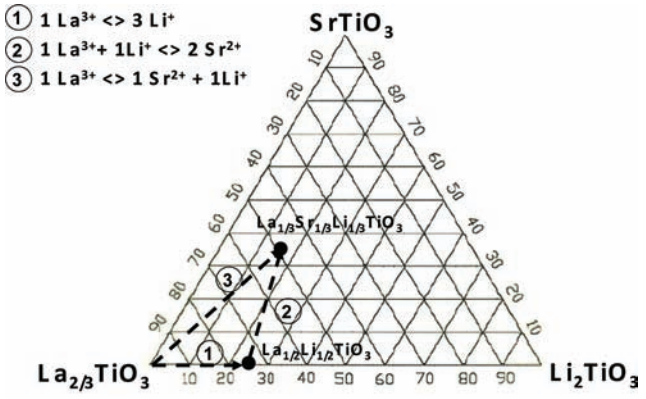

Figure 1. $La_{2/3}TiO_3$−$SrTiO_3$−Li_2TiO_3 compositional diagram, illustrating the Sr doping of LLTO pervoskites. Arrow ③ indicates the solid solutions investigated in this paper. Other substitutional schemes previously studied are also considered, ① and ②.

however, the conductivity decreases.[10,11] The substitution of Ti^{4+} by (Al^{3+} + Li^+) reduced both parameters but increased the conductivity, passing through a maximum for 25% of substitution.[12] The substitution of La^{3+} by other trivalent

Received: February 17, 2012
Published: May 7, 2012

 © 2012 American Chemical Society dx.doi.org/10.1021/ic300365q | *Inorg. Chem.* 2012, 51, 5831−5838

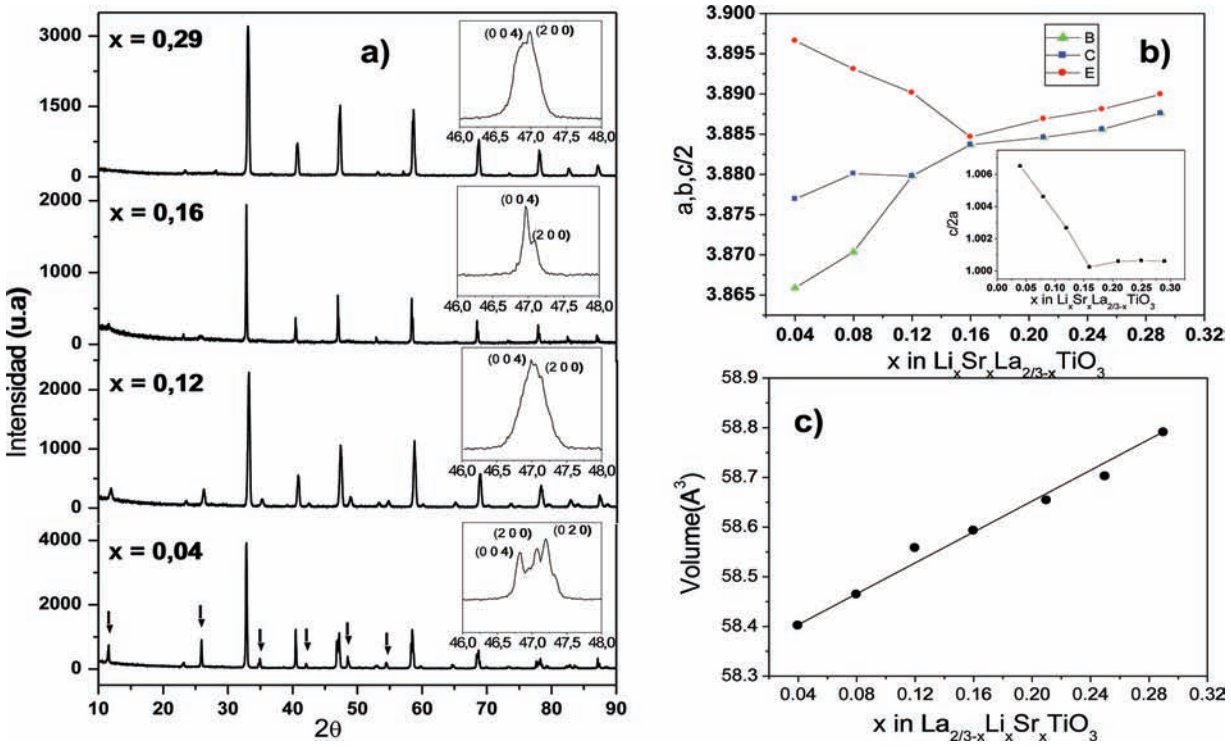

Figure 2. (a) Powder XRD patterns of $Li_xSr_xLa_{2/3-x}TiO_3$ perovskites (x = 0.04, 0.12, 0.16, and 0.29). Superstructure peaks corresponding to doubled perovskites are labeled with arrows. {200} splittings are given as insets. (b) Evolution of lattice parameters versus composition of the samples. The inset indicates the evolution of $c/2a$ ratios. (c) Plot of the unit cell volume versus strontium (or lithium) contents.

rare-earth cations with lower ionic radii, like Nd, Pr, or Sm, keeps constant the number of vacant A sites, but the ionic conductivity decreases as a consequence of the oxygen square-window size decrement produced by contraction of the perovskite unit cell.[13]

On the other hand, low-temperature neutron diffraction experiments showed that Li ions are located at oxygen square windows of LLTO perovskites;[14] the total amount of vacancies participating in lithium conductivity is given by n_t= Li + $\square_A$, the second term standing for nominal vacancies at A sites. The substitution of Li by Na in $Li_{3x}La_{2/3-x}TiO_3$ samples with x = 0.06 and 0.16 did not change the number of nominal $\square_A$ vacancies but decreased the amount of total n_t vacancies, reducing drastically the conductivity when the amount of total vacancy decreased below the percolation threshold of cubic perovskites.[15−17]

The substitution of (La^{3+} + Li^+) by bigger cations like Sr^{2+} in the $Li_{0.5-x}Sr_{2x}La_{0.5-x}TiO_3$ series (line 2 in Figure 1) did not change the amount of nominal vacancies but decreased the amount of total vacancies. In this series, analysis of the dc-conductivity at 300 K showed the progressive decrement of the conductivity after the small maximum detected at Sr = 0.05.[18,19] In the present work, the $La_{2/3}TiO_3$−$Li_{1/3}Sr_{1/3}La_{1/3}TiO_3$ joint of the ternary phase diagram is analyzed, where La^{3+} is substituted by (Sr^{2+} + Li^+) (line 3 in Figure 1). The $Li_xSr_xLa_{2/3-x}TiO_3$ series has been chosen as a complementary system because the amount of nominal vacancies decreases, but the total amount of vacancies n_t = Li + $\square_A$ remains constant. In this work, the lithium conductivity of slowly cooled samples will be compared with that reported previously in quenched samples.[12] Structural features has been deduced from Rietveld analysis of X-ray diffraction (XRD) patterns, and the lithium mobility have been investigated by ^{7}Li NMR and impedance spectroscopy techniques.

2. EXPERIMENTAL SECTION

Samples of the $Li_xSr_xLa_{2/3-x}TiO_3$ series were prepared by a conventional solid-state reaction, from stoichiometric amounts of Li_2CO_3, La_2O_3, TiO_2, and $SrCO_3$, ground together in an agate mortar and heated to 800 °C during 4 h for decarbonation. Then, reground products were cold-pressed at 150 MPa and heated at 1150 °C for 12 h. Finally, pressed powders were heated again at 1275 °C for 6 h. To minimize lithium losses, the heating rate was decreased to 1 °C/min. In the case of strontium-rich samples, the sintering temperature was reduced to 1250 °C to avoid the adhesion of samples to the alumina crucible.

XRD patterns were recorded with Cu Kα radiation in a Phillips X'Pert diffractometer, equipped with a curved graphite monochromator and (θ/2θ) Bragg−Brentano geometry. The 2θ region analyzed was 10−90°, with a step scan of 0.02 and a counting time of 10 s/step. Crystalline phases and lattice parameters were deduced from power XRD patterns by using the *Fullproof* program (matching profile). The Rietveld technique was used to deduce structural features. In this analysis, orthorhombic, tetragonal, and cubic models were used. In this work, Li ions were not considered and isotropic thermal factors were chosen for La, Ti, and O atoms.

^{7}Li NMR spectra were recorded at room temperature, after irradiation of samples with a single pulse (3 μs), in a Avance-400 Bruker spectrometer working at 155.45 MHz (external magnetic field, 9.4 T). In magic-angle-spinning (MAS) experiments, the rotor was of Andrew type and the spinning frequency 10 kHz. The number of scans was 100. Analysis of the NMR spectra was carried out with *Winfit* (Bruker) software. This program allows the position, line width, and intensity of the components to be determined. From spinning-side-band patterns, quadrupole constants C_Q and η of different components were estimated by a trial-and-error procedure. From the fitting of experimental envelopes, the relative intensities of different components were deduced.

dx.doi.org/10.1021/ic300365q | *Inorg. Chem.* 2012, 51, 5831−5838

Table 1. Structural Models Used in Refinements of Orthorhombic, Tetragonal, and Cubic Perovskites (Lithium Was Not Considered)

	Pmmm (No. 47)		*P4/mmm* (No. 123)		*Pm3m* (No. 221)	
atom	position	atomic coordinates	position	atomic coordinates	position	atomic coordinates
La1	1a	0, 0, 0	1a	0, 0, 0	1b	$^1/_2$, $^1/_2$, $^1/_2$
La2	1c	0, 0, $^1/_2$	1b	0, 0, $^1/_2$		
Ti	2t	$^1/_2$, $^1/_2$, $z \approx {}^1/_4$	2h	$^1/_2$, $^1/_2$, z	1a	0, 0, 0
O1	1h	$^1/_2$, $^1/_2$, $^1/_2$	4i	0, $^1/_2$, z	3d	$^1/_2$, 0, 0
O2	2r	0, $^1/_2$, $z \approx {}^1/_4$	1c	$^1/_2$, $^1/_2$, 0		
O3	2s	$^1/_2$, 0, $z \approx {}^1/_4$	1d	$^1/_2$, $^1/_2$, $^1/_2$		
O4	1f	$^1/_2$, $^1/_2$, 0				

Table 2. Structural Parameters Deduced from Powder XRD Data of $La_{2/3-x}Sr_xLi_xTiO_3$ Perovskites[a]

	x									
	0.04 (O)	0.08 (O)	0.12 (T)	0.16 (T)	0.21 (T)	0.21 (C)	0.25 (T)	0.25 (C)	0.29 (T)	0.29 (C)
a	3.8659(1)	3.8703(1)	3.8798(1)	3.8837(2)	3.8846(1)	3.8853(1)	3.8856(1)	3.8864(1)	3.8876(1)	3.8885(1)
b	3.8770(1)	3.8800(1)	3.8798(1)	3.8837(2)	3.8846(1)	3.8853(1)	3.8856(1)	3.8864(1)	3.8876(1)	3.8885(1)
c	7.7932(2)	7.7860(2)	7.7803(3)	7.7693(8)	7.7738(1)	3.8853(1)	7.7762(1)	3.8864(1)	7.7799(1)	3.8885(1)
La1	0.870(3)	0.804(3)	0.741(2)	0.652(3)	0.542(2)		0.440(2)		0.401(2)	
La2	0.384(4)	0.356(4)	0.353(2)	0.362(3)	0.371(2)		0.393(2)		0.352(2)	
Sr1	0.065(3)	0.056(3)	0.154(2)	0.189(3)	0.208(4)		0.268(4)		0.283(3)	
Sr2	0.015(4)	0.024(5)	0.086(2)	0.131(3)	0.212(4)		0.232(4)		0.297(3)	
Ti *z*	0.2599(1)	0.2592(1)	0.2582(1)	0.2549(1)	0.2507(1)		0.2504(1)		0.2504(1)	
O3 *z*	0.2486(3)	0.2492(2)	0.2411(2)	0.2475(1)	0.2530(1)		0.2504(1)		0.2505(1)	
O4 *z*	0.2261(3)	0.2324(3)								
d(Ti–O1)	2.0254(1)	2.0184(1)	2.0087(4)	1.9807(2)	1.9491(1)	1.9427(1)	1.9470(2)	1.9432(1)	1.9484(2)	1.9442(1)
d(Ti–O2)	1.8712(1)	1.8746(1)	1.8814(1)	1.9039(2)	1.9378(1)		1.9411(2)		1.9415(2)	
d(Ti–O3)	1.9349(1)	1.9367(1)	1.9445(1)	1.9427(1)	1.9424(1)		1.9428(1)		1.9438(1)	
d(Ti–O4)	1.9562(1)	1.9512(1)								
R_p	13.2	11.4	13.3	13.7	5.94	5.40	6.02	5.48	6.87	8.38
R_{wp}	16.8	16.3	17.8	18.1	8.71	7.25	8.19	7.59	9.93	13.8
χ^2	3.07	2.04	1.76	1.47	3.14	2.18	2.47	2.14	3.71	7.21
R_B	12.8	9.21	8.77	12.5	4.20	3.45	6.97	3.82	7.73	4.00
R_F	9.59	7.54	7.79	11.5	9.11	2.61	6.41	2.33	7.38	2.91

[a] R_p, R_{wp}, χ^2, and R_B are the conventional agreement factors given by the refinement program.

For conductivity measurements, 12-mm-diameter and 1-mm-thickness pellets were prepared by uniaxial pressing and sintered at 1200 °C for 6 h. In heating and cooling treatments, 1 °C/min thermal ramps were used. In all cases, the relative density of prepared samples was near 90%. In the larger faces of the pellet, ion-blocking gold paste electrodes (Dupont QG150) were deposited. Prepared pellets were heated up to 850 °C for 1 h and then slowly cooled to room temperature. For electric characterization of the samples, a 10 K step was chosen in the 90–480 K range, using a Janis VPF700 cryostat coupled to a LakeShore 331 temperature controller. The electric behavior of the materials was studied using an automatically controlled Agilent Precision LCR E4980-A in the frequency range of 20 Hz to 2 MHz. All of the measurements were performed in a vacuum or an inert atmosphere. Nonlinear least-squares fittings of impedance data were performed with the *ZView2* program.

3. RESULTS AND DISCUSSION

Figure 2a shows the powder XRD patterns, recorded at room temperature, of several $Li_xSr_xLa_{2/3-x}TiO_3$ samples. Along the series, no secondary phases were detected below $x = 0.21$, but for higher lithium contents, very small quantities of an unidentified secondary phase were detected by XRD and scanning electron microscopy (SEM) techniques, which was free of lanthanum as deduced by energy-dispersive spectrometry (EDS) analysis. In analyzed samples, the amount of La ion decreases from 0.66 to 0.33 per structural formula. In the end member of the series, $La_{1/3}Sr_{1/3}Li_{1/3}TiO_3$, similar amounts of La, Sr, and Li cations were incorporated in the perovskite.

All samples display XRD patterns of perovskites; for $x > 0.16$, samples were indexed with the primitive cubic unit cell ($a_p \times a_p \times a_p$), but for $x \leq 0.16$, they were indexed with a doubled perovskite ($a_p \times a_p \times 2\,a_p$) with two different symmetries. For $x < 0.08$, {200} splittings characteristic of orthorhombic perovskites (space group *Pmmm*) were detected (inset of Figure 2a). In the case of samples with $0.08 < x < 0.16$, the symmetry changes to tetragonal (space group *P4/mmm*). For samples with $x > 0.16$, superstructure peaks, related to the *c*-axis doubling, disappeared. The superlattice reflections, marked with arrows, are broader than those of the cubic sublattice and their intensity decreases with the strontium content, indicating that a progressive cation disordering is produced. In similar compositions quenched from the synthesis temperature,[12] structural features differ from those described in this work. On the basis of transmission electron microscopy determinations, authors concluded that the symmetry remains orthorhombic ($\sqrt{2}a_p \times \sqrt{2}a_p \times 2a_p$) in all samples.

In agreement with the ionic radii of elements, the unit cell volume increases with the strontium content (Figure 2c). In Figure 2b, the dependence of unit cell parameters on the lithium content is displayed: the *a* and *b* parameters increase

dx.doi.org/10.1021/ic300365q | Inorg. Chem. 2012, 51, 5831–5838

with the strontium content, while the c axis decreases. Above x = 0.16, the c axis increases in the same manner as the a and b parameters. Finally, the $c/2a$ ratio decreases from 1.006 to 1 as the lithium content increases ($0 < x < 0.16$). For lithium (strontium)-rich cubic samples ($x \geq 0.16$), the $c/2a$ ratio values remain close to 1 (inset of Figure 2b).

Rietveld refinement of the XRD patterns was performed considering *Pm*3*m*, *P*4/*mmm*, and *Pmmm* structural models proposed in the literature[3,7,20,21] for strontium-free samples (Table 1). In this analysis, lithium was not considered because of its low scattering factor. In structural refinements, lanthanum and strontium contents were constrained to nominal compositions. Structural parameters obtained are given in Table 2. For lower lithium compositions, La ions exhibit a clear preference for La1 (0, 0, 0) sites, which decreases when the lithium content increases (Figure 3a). The amount of

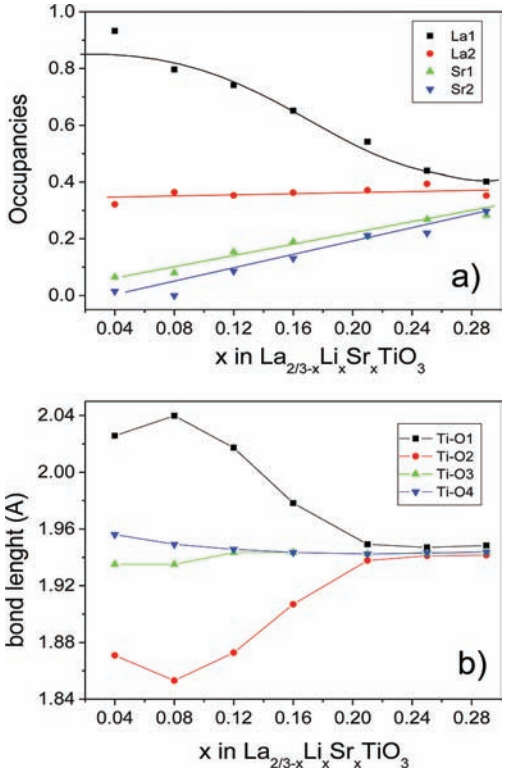

Figure 3. (a) Lanthanum and strontium occupancies of structural sites in $Li_xSr_xLa_{2/3-x}TiO_3$ perovskites. (b) Evolution of Ti−O bond distances as a function of the strontium (or lithium) content. Solid lines are a guide for the eye.

lanthanum in La2 positions (0, 0, $^1/_2$), however, remains basically constant along the series. Regarding the Sr ions, the two site occupancies increase gradually as the strontium content increases, but no preference for any specific site was detected.

In ordered lithium-poor samples ($x \leq 0.04$), lanthanum and vacancies are asymmetrically distributed in alternating planes along the c axis. From this fact, one of the Ti−O distances becomes shorter, while the other becomes longer, producing octahedral distortion along the c axis (Figure 3b). This behavior was first reported in the $La_{2/3-x}$ $Li_{3x}TiO_3$ series,[20,22−24] where vacancies were disposed in alternating planes. For $x > 0.16$ samples, vacancies become disordered, polyhedra become regular, and all Ti−O distances approach 1.95 Å. At intermediate compositions, octahedral distortions associated with vacancy ordering are progressively eliminated.

^{7}Li NMR spectra ($I = {}^3/_2$) are formed by the central ($-{}^1/_2$, ${}^1/_2$) and by two (${}^1/_2$, ${}^3/_2$) and ($-{}^1/_2$, $-{}^3/_2$) satellite transitions. In order to attenuate dipolar Li−Li interactions that broaden NMR spectra, samples were rotated around an axis inclined 54°44′ with respect the external magnetic field (MAS technique). As a consequence of the rotation, the MAS NMR spectra of the $Li_xSr_xLa_{2/3-x}TiO_3$ series displayed a set of narrow equally spaced bands (Figure 4a), which reproduces the

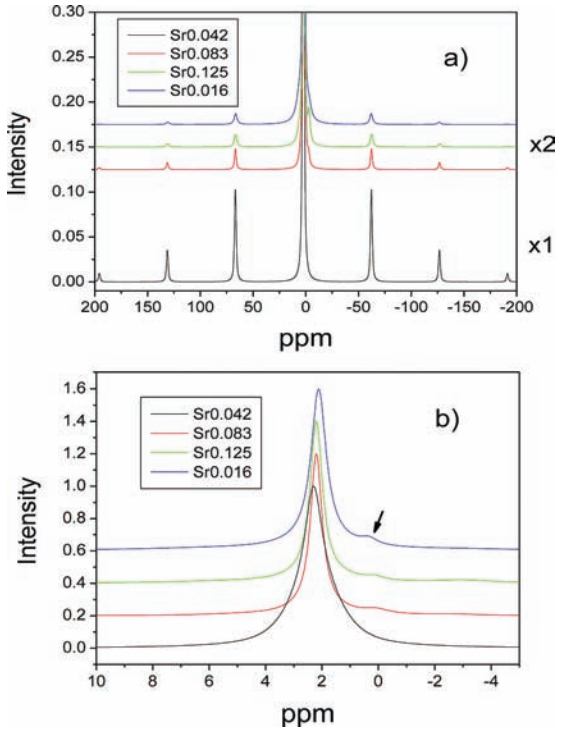

Figure 4. (a) Room temperature ^{7}Li NMR spectra of $Li_xSr_xLa_{2/3-x}TiO_3$ samples with different strontium contents. (b) Expansion of the central part of the spectrum. The shoulder denoted with an arrow has been ascribed to the presence of a La-free impurity (see text).

experimental envelope of static samples. From analysis of these patterns, quadrupole C_Q and η parameters were deduced. In the lithium-poor x = 0.04 sample, the spectrum was reproduced with a single side-band pattern. In lithium-rich samples, quadrupole interactions slightly decrease and a new central component is detected. This band corresponds to Li ions displaying higher mobility. At intermediate compositions, the amount of mobile species increases at the expense of fixed species, increasing the intensity of the central component.

The fitting of spectral envelopes showed the presence of two components at 2.2 ppm, which were ascribed to mobile Li ions (C_Q = 0 kHz; η = 0) and Li ions occupying distorted sites (C_Q = 30 kHz; η = 0.5), displaying a lower mobility. For the sample x = 0.04, the relative intensities of two species were 30 and 70%. In the case of the x = 0.08 sample, quadrupole parameters of the second type of lithium were slightly higher (C_Q = 40 kHz; η = 0.5), but the percentage of mobile species increased up to 70%. For samples with $x \geq 0.08$, an additional component at 0 ppm was detected and was ascribed to the presence of a small amount of the lanthanum-free secondary phase detected by SEM/EDS inspection.

dx.doi.org/10.1021/ic300365q | *Inorg. Chem.* 2012, 51, 5831−5838

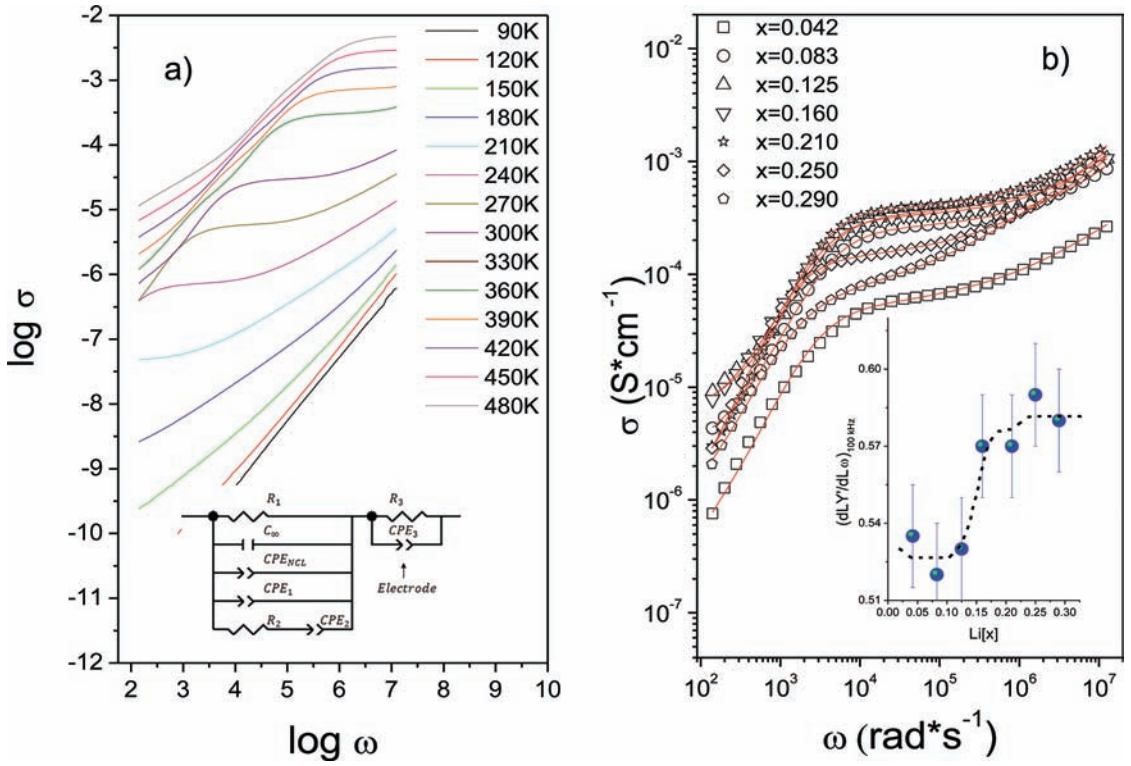

Figure 5. (a) Frequency and temperature dependences of the conductivity of the $Li_{0.125}Sr_{0.125}La_{0.54}TiO_3$ sample. In the inset, the equivalent circuit used for the fitting of data is included. (b) Frequency dependence of the conductivity of $Li_xSr_xLa_{2/3-x}TiO_3$ perovskites at 300 K. The red lines correspond to calculated values (see the text). In the inset, the value of the dispersion parameter n, deduced at 220 K for different compositions, is depicted. The dotted line is a guide for the eye.

In the lithium-poor sample ($x = 0.04$), two detected ^{7}Li MAS NMR signals have been ascribed to lithium species occupying alternating planes of the perovskite. The signal displaying the highest mobility was assigned to Li ions located at $z/c = 0.5$ and that displaying a lower mobility to Li ions located at $z/c = 0$ planes. In the first case, mobility is favored by the presence of A-site vacancies; in the second case, Li ions occupying non-defective layers display lower mobility. The absence of exchange processes between both components allows the determination of two site occupancies. When the relative intensities of two components (30 and 70%) were compared with the amount of vacancy in two planes, it was concluded that occupation by Li ions of vacancy-poor layers is favored in lithium-poor samples. Similar results were reported previously in the $Li_{0.2}La_{0.6}TiO_3$ perovskite; however, in this sample, exchange processes between two species make structural analysis of the Li-site occupancy difficult.[3]

In which concerns conductivity measurements, all samples displayed a similar behavior. As an example, Figure 5a shows the frequency dependence of the real part of the conductivity of $Li_{0.125}Sr_{0.125}La_{0.54}TiO_3$ at different temperatures. It can be seen that a dc plateau ascribed to the bulk contribution is detected above 210 K in a wide temperature range. At higher temperatures, the decay of the conductivity observed at low frequency was ascribed to the blocking of the "bulk" conductivity at grain boundaries. At low temperatures, the constant loss regime, previously reported, was detected (slope near 1).[25] The equivalent circuit, used in analysis of the electrical response of the samples, was based on the blocking model proposed by Dessemond et al.,[26] which is displayed in the inset of Figure 5a. By fitting of the experimental data to this model, the complex conductivity of the grain boundary and bulk contributions were deduced. The bulk conductivity (Figure 5b) adopts the form $\sigma_{dc} + B(i\omega)^n$, where n describes the strength of the conductivity dispersion. In the fitting, the term $A\omega^p$ was considered in parallel with the bulk response, to take into account the presence of the constant loss regime ($p \sim 1$) detected at lower temperatures. In analyzed samples, the exponent n of the bulk contribution is near 0.53 for lithium-poor samples ($0.045 \leq x \leq 0.125$) and 0.58 for lithium-rich samples ($0.16 \leq x \leq 0.29$), with a step between $x = 0.125$ and 0.160 (see inset of Figure 5b).

The temperature dependence of the bulk dc ionic conductivity is given in Figure 6. The maximum difference in the conductivity along the series is 0.83 orders of magnitude. In the inset of this figure, evolution of the conductivity, measured at room temperature, is displayed as a function of the amount of lithium. A maximum of the conductivity is observed at intermediate compositions, $x \sim 0.12$. In all cases, lithium motion was thermally activated, with activation energies going from 0.35 to 0.38 eV along the series. In these samples, the activation energy, E_a, decreased as the temperature increased. The departure of the conductivity from the Arrhenius behavior has been ascribed previously to modifications on lithium motion correlations.[27] In quenched samples, the "bulk" conductivity was slightly larger, with a maximum in the conductivity for lithium contents near 0.25. The activation energy values reported in quenched samples[12] are similar to those obtained in slowly cooled samples (this work).

In order to study the compositional dependence of the conductivity, preexponential factors of the conductivity were analyzed. In Figure 7, normalized preexponential factor (σ_0/

dx.doi.org/10.1021/ic300365q | Inorg. Chem. 2012, 51, 5831−5838

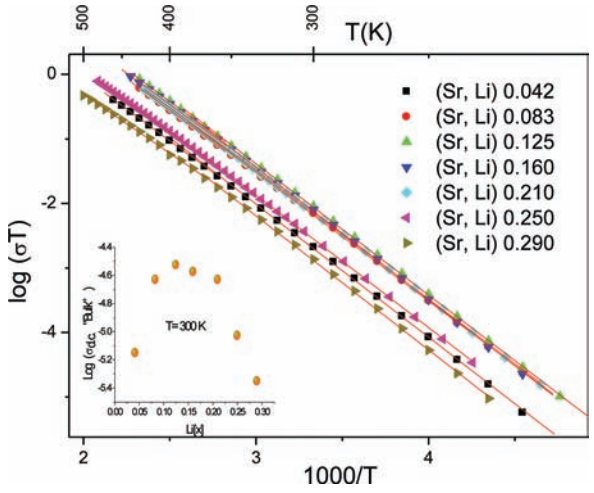

Figure 6. Temperature dependence of the conductivity of $Li_xSr_xLa_{2/3-x}TiO_3$ samples. In the inset, evolution of the room temperature conductivity as a function of the lithium (or strontium) content is displayed.

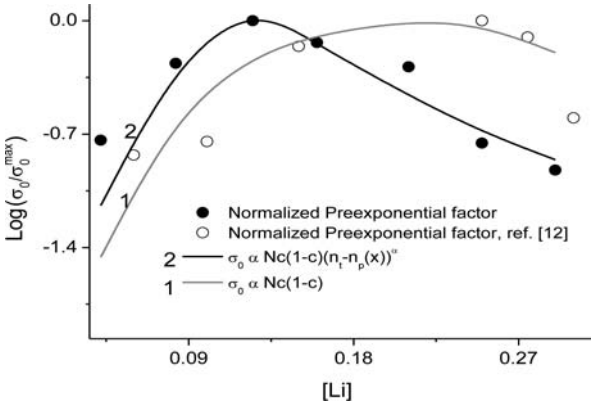

Figure 7. Preexponential factors (deduced experimentally from conductivity data) versus lithium content, calculated in slowly cooled samples (bold symbols). Data corresponding to quenched samples taken from ref 12 are indicated by open symbols. Calculated values for two distribution models considered in this work are also given (solid lines 1 and 2).

σ_0^{max}) values, extrapolated from the linear conductivity plots detected between 250 and 330 K, are displayed as a function of the lithium content for slowly cooled samples and for quenched samples analyzed in ref 12.

In general, preexponential factors can be expressed as

$$\sigma_0 = f(Nq^2)(l^2\omega_0/r)c(1-c)/k \exp(\Delta S_m/k) \quad (1)$$

where q and N are the charge and concentration of charge carriers, l is the distance to the nearest-neighbor equivalent sites ($r \leq 6$), having the probability c of being occupied by mobile Li ions and the probability 1 - c of being empty. In this expression, ω_0 is the attempt frequency, f is a structural correction factor (near unity), k is the Boltzmann constant, and ΔS_m is the entropy change associated with the lithium migration.

In expression (1), the probability for lithium hopping between contiguous sites is given by the $c(1-c)$ product. In analyzed samples, two types of cation vacancies can be considered: (1) vacancies located at A sites and (2) vacancies located at square windows that surround A sites of perovskites.

In this work, two cation/vacancy distributions have been considered:

(1) The random distribution of lithium and vacancy at square windows that surround A sites of the perovskite. In this model, vacant A sites do not contribute to the conductivity. In this case, the amount of lithium and vacant sites per structural site will be $x/3$ and $(3-x)/3$, and its contribution to the conductivity will be given by $x(3-x)/9$. The resulting maximum observed on the conductivity should be out of the explored compositional range ($x = 1.5$). This prediction was not observed, disregarding its contribution to dc-conductivity. The lithium motion between equivalent square windows of the same unit cell could be responsible for the constant loss contribution.

(2) Lithium hopping is only possible when contiguous A sites are vacant, preventing occupation of the same unit cell with two Li ions. In this case, the amount of lithium and nominal vacancies, related by lithium hopping between contiguous cells, is x and $(^1/_3 - x)$. In this model, local motions of lithium between equivalent square windows of the same unit cell do not contribute to the dc conductivity. On these bases, a maximum of $c(1-c)$ should be detected at $x = 0.16$. Taking into account that the preexponential factor is proportional to $Nc(1-c)$ (see eq 1), the maximum is shifted to $x = 0.21$ (line 1 in Figure 7), near that experimentally observed in quenched samples.[25]

In slowly cooled samples, the distribution of vacancies in different structural phases must also be considered. In order to analyze the influence of this factor on the dc conductivity, values reported in the $Li_{3x}La_{2/3-x}TiO_3$ (LLTO), $(Li_{1-x}Na_x)_{0.5}La_{0.5}TiO_3$ (LNLTO.5), and $(Li_{1-x}Na_x)_{0.2}La_{0.6}TiO_3$ (LNLTO.6) series were analyzed on the basis of the percolation model of vacancies[17] (Figure 8). In this analysis, conductivity values were fitted to the expression

$$\sigma_{dc} = K(n_t - n_p)^{\alpha} \quad (2)$$

where n_p is the percolation threshold and n_t stands now for the sum of nominal vacancies plus the lithium content, Li + $\square_A$. In this model, A sites associated with Li ions favor the lithium conductivity, meanwhile A sites occupied by Na, Sr, and La ions block lithium diffusion.[17] In Figure 8a, conductivity values of the analyzed series are plotted as a function of n_t. It is observed that the $Li_xSr_xLa_{2/3-x}TiO_3$ results are near those reported previously in LNLTO.5, confirming that the amount of total vacancy, n_t = Li + $\square_A$ = 0.33, remains above the percolation threshold of perovskites. However, to explain the decrease observed in the conductivity (Figures 7 and 8a), differences in the percolation threshold (dimensionality of the conductivity) should be considered.

The NMR spectra of lithium-poor $Li_xSr_xLa_{2/3-x}TiO_3$ (x = 0.04 and 0.08) samples have shown the presence of vacancy ordering and a considerable amount of lithium that displays low mobility. The absence of exchange processes between two crystallographic planes indicates that the dimensionality of the conductivity in lithium-poor samples should be lower than that of lithium-rich ones. If only mobile Li ions are taken into account in calculations of vacant n_t sites, conductivity values of $Li_xSr_xLa_{2/3-x}TiO_3$ are located between those of the LNLTO.6 and LNLTO.5 series, displayinig 2D and 3D lithium conductivity (see Figure 8a). This observation suggests that the percolation threshold of this series changes from 2D (n_p = 0.27) to 3D (n_p= 0.31) as the lithium content increases. It should be noted that the 2D percolation threshold, n_p = 0.27, is

dx.doi.org/10.1021/ic300365q | Inorg. Chem. 2012, 51, 5831−5838

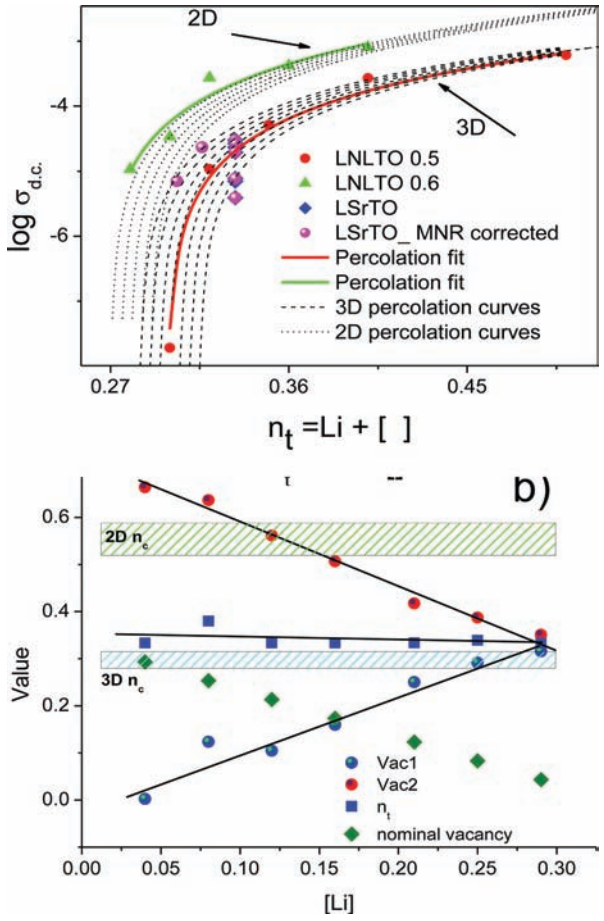

Figure 8. (Top) Plot of room temperature dc conductivity versus total amount of vacancy, n_t, in different series: $Li_xSr_xLa_{2/3-x}TiO_3$ (blue diamonds), $(Li_{1-x}Na_x)_{0.2}La_{0.6}TiO_3$ (green triangles), and $(Li_{1-x}Na_x)_{0.5}La_{0.5}TiO_3$ (red circles). Pink circles correspond to n_t values after subtraction of nonmobile lithium species deduced by NMR. 3D and 2D conductivity curves calculated for different thresholds are given as dashed and dotted lines. (Bottom) Vacancy concentration at two structural sites (Vac1 and Vac2) deduced by Rietveld analysis from XRD patterns. The variations of nominal ($\square_A$) and total (n_t) vacancies are also depicted.

determined in the same unit cell volume as that used in 3D threshold determination.

The change of the dimensionality should be related to variations observed on the distribution of $\square_A$ vacancies along the $Li_xSr_xLa_{2/3-x}TiO_3$ series. As mentioned before, the incorporation of strontium decreases the amount of La1 but has almost no affect on that of La2 in analyzed perovskites (see Figure 3a). From structural analysis carried out in analyzed samples, the amount of vacancies at (0, 0, 0) and (0, 0, $^1/_2$) planes was estimated. In Figure 8b, the amount of vacancies in both planes is given as a function of the lithium content. In doubled perovskites, averaged values, $n_t = (\square_{A1} + \square_{A2})/2$, are near the percolation threshold of cubic perovskites; however, the percolation threshold of vacant-rich planes should change from 2D ($0.5 < n_p < 0.59$) to 3D ($0.31 < n_p < 0.33$) values in the crystal cell as the amount of strontium (lithium) increases.

Further evidence for changes in the dimensionality of the ionic conductivity came from the step variation detected at $x \sim 0.16$ on the exponent of the frequency dependence of the conductivity. A change of the dimensionality from 2D to 3D produces an increment on the n values similar to that observed, from 0.53 to 0.58, in analyzed samples.[28] The observation of this step was produced when vacant-site concentrations in vacancy-rich planes drop below the 2D percolation threshold (Figure 8b). Similar observations were reported in the $(Li,Na)_{3x}La_{2/3-x}TiO_3$ series when the percolation threshold of ordered ($x = 0.2$) and disordered ($x = 0.5$) samples were compared.

If percolation processes are taken into account, the preexponential factor of the conductivity should be proportional to $c(1 - c)(n_t - n_p(x))^2$ (plot 2 in Figure 7).[16] In our case, it has been considered that $n_p(x)$ is 0.28 for orthorhombic samples, increasing from $n_p = 0.29$ to 0.31 when the dimensionality of the conductivity increases. In this analysis, $c = Li^*/[Li^* + \square_A]$ and $1 - c = \square_A/[Li^* + \square_A]$, with Li* being the fraction of mobile ions deduced from NMR experiments to calculate conductivity preexponential factors (see line 2 in Figure 7).

In quenched $Li_xSr_xLa_{2/3-x}TiO_3$ samples, conductivity values are reasonably well reproduced when lithium hopping between contiguous cells is controlled by lithium and nominal vacancy concentrations. In these samples, the contribution of the percolation factor is constant along the series. However, in slowly cooled samples, the understanding of the dc conductivity requires consideration of the ordering of vacancies. The changes produced in vacancy ordering are responsible for modifications of the dimensionality and the corresponding percolation thresholds. This variation is responsible for the shift of the maximum of the preexponential factor from $x = 0.22$ to 0.12.

4. CONCLUSIONS

The structural evolution of slowly cooled A-site deficient $Li_xSr_xLa_{2/3-x}TiO_3$ perovskites ($0.04 \leq x \leq 0.29$) has been studied. The substitution of the La ion by (Sr + Li) reduces the amount of nominal vacancies but maintains constant the total amount of vacancies, n_t, that participate in conduction processes. In doubled perovskites ($x < 0.16$), the symmetry changes from orthorhombic to tetragonal when the lithium content increases above $x = 0.08$. For samples with $x > 0.16$, a pseudocubic symmetry was detected. La ions and vacancy-rich planes alternate in successive planes along the c axis in lithium-poor perovskites, but vacancies become disordered in lithium-rich samples.

^{7}Li NMR spectra are mainly formed by two components that have been assigned to lithium species located at $z/c = 0$ and $z/c = 0.5$ planes, both displaying different mobilities. The preferential occupation of $z/c = 0$ favors the 2D lithium mobility; however, the progressive occupation of $z/c = 0.5$ planes enhances exchange processes between two planes, favoring the 3D mobility. Information deduced by NMR indicates that the percentage of mobile Li ions that participate in the conductivity is lower than nominal ones in orthorhombic samples. Lithium motion was thermally activated, with activation energies going from 0.35 to 0.38 eV. The maximum observed in preexponential factors of the conductivity is related to the charge carriers and vacancy concentration. Changes on the vacancy ordering modify the dimensionality of the conductivity, indicating that not only the amount of vacancies but also its distribution is relevant. The maximum of preexponential factors shifts toward lower lithium contents in slowly cooled samples.

dx.doi.org/10.1021/ic300365q | Inorg. Chem. 2012, 51, 5831−5838

AUTHOR INFORMATION

Corresponding Author
*E-mail: jsanz@icmm.csic.es.

Notes
The authors declare no competing financial interest.

ACKNOWLEDGMENTS

The authors are thankful for financial support received from MICINN (Project MAT2010-19837-CO6) and regional CAM government (Program MATERYENER S2009 PPQ-1626). W.B. thanks the Spanish MICINN Ministry for a predoctoral grant.

REFERENCES

(1) Inaguma, Y.; Chen, L.; Itoh, M.; Nakamura, T.; Uchida, T.; Ikuta, H.; Wakihara, M. *Solid State Commun.* **1993**, *86*, 689.
(2) Belous, A. G.; Novitskaya, G. N.; Polyanetskaya, S. V.; Gornikov, Y. I. *Zh. Neorg. Khim.* **1987**, *32*, 283.
(3) Paris, M. A.; Sanz, J.; León, C.; Santamaría, J.; Ibarra, J.; Varez, A. *Chem. Mater.* **2000**, *12*, 1694.
(4) Inaguma, Y.; Katsumata, T.; Itoh, M.; Morii, Y. *J. Solid State Chem.* **2002**, *166*, 67.
(5) Ruiz, A. I.; López, M. L.; Veiga, M. L.; Pico, C. *Solid State Ionics* **1998**, *112*, 291.
(6) Harada, Y.; Hirakoso, Y.; Kawai, H.; Kuwano, J. *Solid State Ionics* **1999**, *121*, 245.
(7) Ibarra, J.; Varez, A.; León, C.; Santamaría, J.; Torres-Martinez, L.; Sanz, J. *Solid State Ionics* **2000**, *134*, 219.
(8) Varez, A.; Ibarra, J.; Rivera, A.; León, C.; Santamaría, J.; Laguna, M. A.; Sanjuán, M. L.; Sanz, J. *Chem. Mater.* **2003**, *15*, 225.
(9) Stramare, S.; Thangadurai, V.; Weppner, W. *Chem. Mater.* **2003**, *15* (21), 3974.
(10) Kawakami, Y.; Ikuta, H.; Wakihara, M. *J. Solid State Electrochem.* **1998**, *2*, 206−.
(11) Garcia-Martin, S.; Rojo, J. M.; Tsukamoto, H.; Moran, E.; Alario-Franco, M. A. *Solid State Ionics* **1999**, *116*, 11−.
(12) Morata-Orrantia, A.; Garcia-Martin, S.; Moran, E.; Alario-Franco, M. A. *Chem. Mater.* **2002**, *14* (7), 2871−.
(13) Itoh, M.; Inaguma, Y.; Jung, W. H.; Chen, L.; Nakamura, T. *Solid State Ionics* **1994**, *70*−*71*, 203−.
(14) Alonso, J. A.; Sanz, J.; Santamaría, J.; León, C.; Varez, A.; Fernandez-Diaz, M. T. *Angew. Chem., Int. Ed* **2000**, *3*, 619.
(15) Rivera, A.; León, C.; Santamaria, J.; Varez, A.; V'yunov, O.; Belous, A. G.; Alonso, J. A.; Sanz, J. *Chem. Mater.* **2002**, *14*, 5148.
(16) Inaguma, Y.; Itoh, M. *Solid State Ionics* **1996**, *86*−*88*, 257−.
(17) Herrero, C. P.; Varez, A.; Rivera, A.; Santamaría, J.; León, C.; V'yunov, O.; Belous, A. G. *J. Phys. Chem. B* **2005**, *109*, 3262−.
(18) Inaguma, Y.; Chen, L.; Itoh, M.; Nakamura, T. *Solid State Ionics* **1994**, *70*−*71*, 196−.
(19) Wang, G. X.; Yao, P.; Bradhurst, D. H.; Dou, S. X.; Liu, H. K. *J. Mater. Sci.* **2000**, *35*, 4289.
(20) Kim, I. S.; Nakamura, T.; Inaguma, Y.; Itoh, M. *J. Solid State Chem.* **1994**, *113*, 281.
(21) Mizumoto, K.; Hayashi, S. *J. Ceram. Soc. Jpn.* **1997**, *105*, 713−715.
(22) Abe, M.; Uchino, K. *Mater. Res. Bull.* **1974**, *9*, 147.
(23) McEachen, M. J.; Dabkowska, H.; Garret, J. D.; Amow, G.; Gong, W.; Lio, G.; Greedan, J. E. *Chem. Mater.* **1994**, *6*, 2092.
(24) Sanz, J.; Varez, A.; Alonso, J. A.; Fernandez, M. T. *J. Solid State Chem.* **2004**, *177*, 1157−.
(25) León, C.; Rivera, A.; Varez, A.; Sanz, J.; Santamaría, J. *Phys. Rev. Lett.* **2001**, *86*, 1279.
(26) Dessemond, L.; Muccillo, R.; Henault, M.; Kleitz, M. *Appl. Phys. A: Mater. Sci. Process.* **1993**, *57* (1), 57−.
(27) Jimenez, R.; Rivera, A.; Varez, A.; Sanz, J. *Solid State Ionics* **2009**, *180*, 1362−.
(28) Sidebottom, D. L. *Phys. Rev. Lett.* **1999**, *83* (5), 983−.